OXFORD

*Journal of Petrology*, 2024, **65**, egae119
https://doi.org/10.1093/petrology/egae119
ADVANCE ACCESS PUBLICATION DATE 7 NOVEMBER 2024
**Original Manuscript**

# Depths in a Day—a New Era of Rapid-Response Raman-Based Barometry Using Fluid Inclusions

CHARLOTTE L. DEVITRE[1,*], PENNY E. WIESER[1], ALEXANDER T. BEARDEN[1], ARAELA RICHIE[1], BERENISE RANGEL[1], MATTHEW L.M. GLEESON[1], JOHN GRIMSICH[1], KENDRA J. LYNN[2], DREW T. DOWNS[2], NATALIA I. DELIGNE[2] and KATHERINE M. MULLIKEN[2]

[1]Earth and Planetary Science, University of California, Berkeley, McCone Hall, Berkeley, CA 94270, USA
[2]Hawaiian Volcano Observatory, U. S. Geological Survey, Kamehameha Avenue, Hilo, HI 96720, USA

*Corresponding author. E-mail: cl.devitre@gmail.com

Rapid-response petrological monitoring is a major advance for volcano observatories, allowing them to build and validate models of plumbing systems that supply eruptions in near-real time. The depth of magma storage has recently been identified as high-priority information for volcanic observatories, yet this information is not currently obtainable via petrological monitoring methods on timescales relevant to eruption response. Fluid inclusion barometry (using micro-thermometry or Raman spectroscopy) is a well-established petrological method to estimate magma storage depths and has been proposed to have potential as a rapid-response monitoring tool, although this has not been formally demonstrated. To address this deficiency, we performed a near-real-time rapid-response simulation for the September 2023 eruption of Kīlauea, Hawai'i. We show that Raman-based fluid inclusion barometry can robustly determine reservoir depths within a day of receiving samples—a transformative timescale that has not previously been achieved by petrological methods. Fluid inclusion barometry using micro-thermometric techniques has typically been limited to systems with relatively deep magma storage (>0.4 g/cm$^3$ i.e. >7 km) where measurements of $CO_2$ density are easy and accurate because the $CO_2$ fluid homogenizes into the liquid phase. Improvements of the accuracy of Raman spectroscopy measurements of fluids with low $CO_2$ density over the past couple of decades has enabled measurements of fluid inclusions from shallower magmatic systems. However, one caveat of examining shallower systems is that the fraction of $H_2O$ in the fluid may be too high to reliably convert $CO_2$ density to pressure. To test the global applicability of rapid response fluid inclusion barometry, we compiled a global melt inclusion dataset (>4000 samples) and calculate the fluid composition at the point of vapor saturation ($X_{H_2O}$). We show that fluid inclusions in crystal hosts from mafic compositions (<57 wt. % $SiO_2$)—likely representative of magmas recharging many volcanic systems worldwide—trap fluids with $X_{H_2O}$ low enough to make fluid inclusion barometry useful at many of the world's most active and hazardous mafic volcanic systems (e.g. Iceland, Hawai'i, Galápagos Islands, East African Rift, Réunion, Canary Islands, Azores, Cabo Verde).

**Key words**: fluid inclusions; geobarometry; Raman spectroscopy; rapid-response; volcano monitoring

## INTRODUCTION

Volcano observatories increasingly use data collected from erupted lava and tephra samples in near-real time to obtain information about the magmatic plumbing system to help inform decision-making during volcanic crises (Gansecki *et al.*, 2019; Re *et al.*, 2021; Pankhurst *et al.*, 2022). Most studies so far have focused on the chemistry of erupted lavas and their crystal cargoes (Pankhurst *et al.*, 2022) to gain insight into changing melt compositions and rheological properties (Gansecki *et al.*, 2019). Until now, petrological monitoring has been unable to address the high-priority question—*Where is the magma coming from?* (Re *et al.*, 2021). At well-monitored volcanoes, such information can be used to draw analogies to previous eruptive episodes associated with specific storage reservoirs (e.g. vigor, pathway or length of eruption), and to help interpret geophysical signals of ongoing activity. At poorly monitored volcanoes, where there may be no prior constraints on magma storage geometry (Wieser *et al.*, 2023b), depths of storage are a vital parameter to interpret unrest associated with a new episode of eruptive activity (Pritchard *et al.*, 2019). Even at well-monitored volcanoes, the magma chamber supplying a given eruptive episode may be uncertain. For example, the return of eruptive activity at Kīlauea in December 2020 was accompanied by many questions about how the magmatic plumbing system had changed following >500 m of summit caldera collapse in 2018 (Lynn *et al.*, 2024b).

Melt inclusion barometry, a widely popular petrological method to determine storage depths from volatile contents, is slow (Re *et al.*, 2021) often taking months to complete. For example, Lerner *et al.* (2021) and Wieser *et al.* (2021) both published peer-reviewed papers ~3 years after the 2018 lower East Rift Zone eruption of Kīlauea had ended. While mineral barometry can be implemented faster, it is also more imprecise (Wieser *et al.*, 2023a), and therefore can only constrain magma storage to very broad depths (e.g. crust vs sub-Moho). It also has poor applicability at active volcanoes such as Kīlauea or Mauna Loa, where the only major silicate phase in many of their eruptive products is olivine, the chemistry of which is not pressure-sensitive, and where a precision of 1–2 km is needed to distinguish between reservoirs identified by geophysics (Baker & Amelung, 2012; Anderson & Poland, 2016).

**RECEIVED** APRIL 26, 2024; **REVISED** OCTOBER 22, 2024; **ACCEPTED** NOVEMBER 5, 2024
Published by Oxford University Press 2024.

Fluid inclusion barometry via micro-thermometry and Raman spectroscopy is a well-established technique that has regularly been applied to determine the structure of magma plumbing systems over the past four decades (Roedder & Bodnar, 1980; Roedder, 1983, 1984; Belkin *et al.*, 1985; Hansteen *et al.*, 1991; Andersen *et al.*, 1995; Hansteen *et al.*, 1998; Yamamoto *et al.*, 2002; Frezzotti *et al.*, 2003; Klügel *et al.*, 2005; Yamamoto *et al.*, 2007; Bali *et al.*, 2008; Hansteen & Klügel, 2008; Ladenberger *et al.*, 2009; Hildner *et al.*, 2011, 2012; Zanon & Frezzotti, 2013; Levresse *et al.*, 2016; Klügel *et al.*, 2020; Boudoire *et al.*, 2023; Dayton *et al.*, 2023; Zanon *et al.*, 2024). Micro-thermometry—which consists of measuring the temperature at which phase changes occur in a fluid under a microscope—can determine the $CO_2$ density of fluid inclusions with bulk densities above critical (>0.45 g/cm$^3$) with great accuracy (Hansteen & Klügel, 2008; Bakker, 2021). However, it is difficult to observe the evaporation of a thin liquid film in fluid inclusions that homogenize to the vapor phase (Hansteen & Klügel, 2008), and therefore the technique has limited applicability to ability to determine the shallow structure of magmatic plumbing systems (<5–7 km), except perhaps in the case of large fluid inclusions in clear host phases, such as quartz (Clocchiatti *et al.*, 1994; Zanon *et al.*, 2003). Developments over the past two decades in the accuracy and precision of Raman spectroscopy, which uses spectral features of $CO_2$ fluids to calculate a $CO_2$ density using an instrument-specific calibration (Rosso & Bodnar, 1995; Kawakami *et al.*, 2003; Yamamoto & Kagi, 2006; Fall *et al.*, 2011; Wang *et al.*, 2011, 2019; Lamadrid *et al.*, 2017; Sublett *et al.*, 2020; DeVitre *et al.*, 2021; Le *et al.*, 2021), have made it possible to accurately measure lower $CO_2$ densities, and thus identify shallow storage regions more reliably. Recent studies demonstrate that Raman-based barometry of $CO_2$-rich fluid inclusions return the same results as melt inclusion barometry while requiring far less time and resources than melt inclusion analyses, and obtain higher precision than mineral thermobarometry (Dayton *et al.*, 2024; DeVitre & Wieser, 2024; Lerner *et al.*, 2024). Although micro-thermometry is generally more accurate than Raman spectroscopy for high-density $CO_2$ fluids (>0.6 g/cm$^3$; Bakker, 2021), Raman spectroscopy has the advantage of being able to easily measure nearly the entire range of geologically relevant $CO_2$ densities (from very low to high) with reasonably consistent precision and accuracy. It is also possible to assess the composition of the fluids and/or solids in inclusions using Raman spectroscopy. The $CO_2$ density obtained from either technique, along with an estimate of entrapment temperature, is converted into an entrapment pressure using an equation of state (EOS, Fig. 2, either pure $CO_2$ or $CO_2$-$H_2O$).

Recent studies have speculated that fluid inclusion barometry, using either micro-thermometry or Raman spectroscopy, could be performed quickly enough to be useful for near-real-time volcano monitoring (Dayton *et al.*, 2023; Zanon *et al.*, 2024). These speed improvements stem from advances in the accuracy of Raman measurements through two decades of improvements in $CO_2$ densimetry calibrations, along with new capabilities to process data in a more streamlined and reproduceable way (Wieser & DeVitre, 2024). However, the speed of this technique on timescales applicable to eruption response has not been formally demonstrated. The CONVERSE Hawai'i Scientific Advisory Committee (Cooper *et al.*, 2023) specifically recommended that key science questions be identified, and preplanning science activities performed, to facilitate rapid implementation across a broader scientific group during eruptions.

Here, we performed a near-real-time simulation to rigorously assess how quickly fluid inclusion depths can be obtained from erupted material using Raman spectroscopy, and whether these timescales are short enough to have utility as a petrological monitoring tool. We also evaluated the applicability of the method at other volcanic systems worldwide. We focused on Raman spectroscopy given that it is applicable to a wider range of storage depths than micro-thermometry, requires less sample preparation, is available at more institutions, and has the capability for easily characterizing the composition of fluids. Performing these simulations during a relatively small, low-hazard eruptions or as a hypothetical simulation (Andrews *et al.*, 2019) is vital to working out any potential bottlenecks so that we are as prepared as possible for the next volcanic crisis (Dietterich & Neal, 2022). Importantly, this simulation revealed that rapid-response fluid inclusion work in collaboration with academic institutions was not taxing on observatory or academic staff (Cooper *et al.*, 2023) and can be employed during future eruptions. Our work also demonstrates the utility of fluid inclusion barometry at many of the world's most active and hazardous mafic volcanic systems.

## Timeline of the rapid-response simulation

The eruption onset of Kīlauea on September 10, 2023, provided an ideal opportunity to test the validity and speed of the fluid inclusion method, given that depths of the two main magma storage regions (Halema'uma'u (HMM) at 1–2 km and south caldera at 3–5 km) at this volcano have been well constrained by various independent geophysical and petrological methods, including prior fluid inclusion barometry (DeVitre & Wieser, 2024; Lerner *et al.*, 2024). Tephra samples representing the first ~14 h of the September 2023 eruption were collected by U.S. Geological Survey Hawaiian Volcano Observatory (HVO) geologists on September 12 and mailed to UC Berkeley on September 15 (Fig. S1). A schematic of the workflow and a detailed timeline are available in the supplement (Fig. S1).

Our simulation started on September 20 at 9:00 am Pacific Standard Time (PST) (day 1), which is the morning after the samples arrived at UC Berkeley (Fig. S1). We used a production-line-style workflow involving two undergraduates, a first year graduate student, a post-doc and an assistant professor, with stations for crushing and sieving, mineral picking, fluid inclusion preparation, sample cataloging and analysis. We crushed and sieved tephra, picked olivine phenocrysts (size fractions of 0.5–1 and 1–2 mm) and mounted them in CrystalBond™* to search for fluid inclusions. By ~2:00 pm PST, we collected our first Raman spectra, and by ~7:00 pm PST, we had calculated $CO_2$ densities from 16 fluid inclusions using a previously established instrument-specific calibration of the relationship between $CO_2$ density and Fermi diad splitting distance (DeVitre *et al.*, 2021; DeVitre & Wieser, 2024). All spectra processing and subsequent calculations were performed using DiadFit (Wieser & DeVitre, 2024), allowing for a conversion of a day's worth of raw spectra to $CO_2$ densities within ~15 min. Pressures were calculated using the pure $CO_2$ EOS of Span & Wagner (1996) implemented in DiadFit. At the time of our simulation, it was challenging to perform EOS calculations due to the possible presence of $H_2O$ in the exsolved fluid resulting from a lack of publicly available software that can run on modern computer operating systems. However, recent work by Yoshimura (2023) identified errors in the published equations for the $H_2O$–$CO_2$ EOS of Duan & Zhang (2006) and has provided an open-source C code, which after conversion to python, allowed such calculations to be performed in DiadFit. Using estimates of $\mathbf{X}_{H_2O}$ from previously published melt inclusion data at Kīlauea (Wieser *et al.*, 2021; DeVitre & Wieser, 2024), calculated pressures would

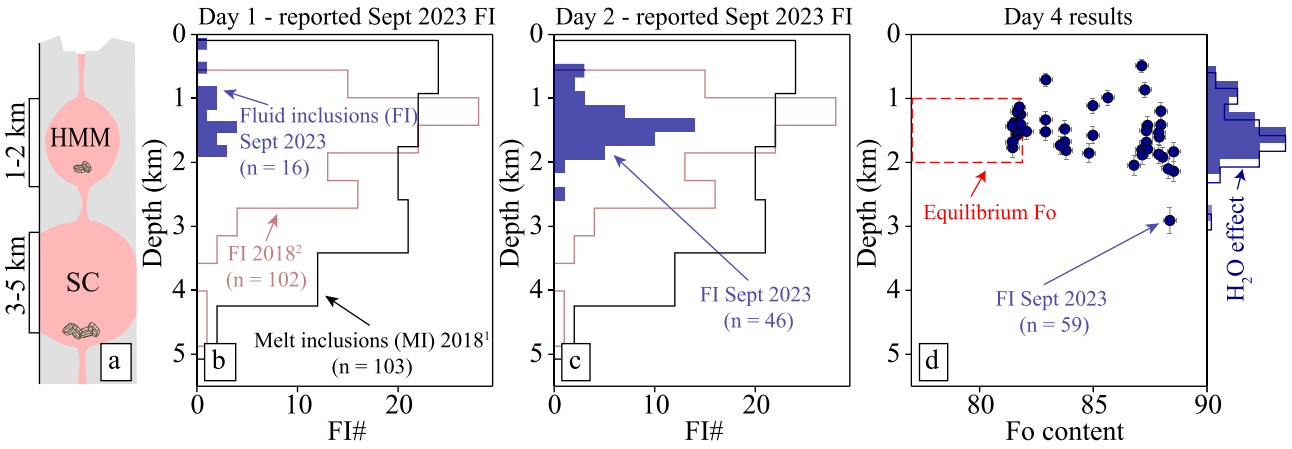


**Fig. 1.** Evolution of results over 4 days. a) Schematic model of Kīlauea's plumbing system, indicating reservoir depths (HMM = Halema'uma'u; SC = south caldera). b) Day 1 fluid inclusion depths, as reported to HVO, are consistent with the estimated depths of the Halema'uma'u reservoir. Kolmogorov–Smirnoff tests indicate that September 2023 fluid inclusions record significantly shallower depths than fluid inclusions (critical D = 0.22, stat = 0.24, *P* value = 0.016) and melt inclusions (critical D = 0.22, stat = 0.41, *P* value = 3.51e-06) from the 2018 lower East Rift Zone eruption, which required a contribution from the south caldera reservoir (Wieser *et al.*, 2021; DeVitre & Wieser, 2024). [1]Lower East Rift Zone 2018 melt inclusions (Wieser *et al.*, 2021); [2] Lower East Rift Zone 2018 fluid inclusions (DeVitre & Wieser, 2024). c) Day 2 data confirmed a likely dominant role for the Halema'uma'u reservoir. A conservative degassing filter was applied ($SO_2/CO_2$ peak ratio < 0.1). d) Day 4 data, means were taken for repeated analyses of single fluid inclusions and additional data filters (e.g. $SO_2/CO_2$ peak ratio < 0.22), fluid inclusion-specific temperatures, and a more appropriate crustal density model (~2300 kg/m$^3$ with a normal error distribution of 100 kg/m$^3$) were applied. Error bars correspond to uncertainties propagated using Monte Carlo simulations and olivine forsterite (Fo = 100*Mg/(Mg+Fe) molar) equilibrium field was calculated based on glass electron probe microanalysis data collected on September 11, 2023 (Lynn *et al.*, 2024a). The shifted histogram '$H_2O$ effect' shows the effect of $H_2O$ corrections on pressures recalculated using $X_{H_2O}$ inferred from melt inclusions (Wieser *et al.*, 2021; DeVitre & Wieser, 2024).

be ~10% higher than originally reported to HVO if the $CO_2$–$H_2O$ EOS had been used (Fig. 1d, Fig. S1 in supplementary materials). This does not affect the interpretation of our results, as the shift is far smaller than the pressure offset between the Halema'uma'u (Fig. 1a 'HMM' at ~1–2 km) and south caldera (Fig. 1a 'SC' at ~3–5 km) reservoir.

For days 1 and 2 of the simulation, we assumed an entrapment temperature of 1150 °C for all fluid inclusions based on geothermometric estimates of previously erupted liquids (Gansecki *et al.*, 2019; DeVitre & Wieser, 2024). On day 4, we calculated entrapment temperatures for each fluid inclusion using the host forsterite content (Fo = 100*Mg/(Mg+Fe) molar; DeVitre & Wieser, 2024) measured by energy dispersive spectroscopy (EDS), yielding temperatures spanning 1182–1307 °C. The average error induced by our initial assumption of 1150 °C is only ~7% (with a maximum offset of only 12%). While crystallization temperatures at Kīlauea are well constrained relative to other volcanic systems, by applying similar regression methods to that of DeVitre & Wieser (2024) to relate liquid compositions to host olivine Fo contents, it should always be possible to constrain temperatures within ~100 K at different volcanic systems using host mineral chemistry.

On days 1 and 2, pressures were converted into depths using the crustal density model of Ryan (1987), as parameterized by Lerner *et al.* (2021). We shared the resulting histogram (Fig. 1a and b) of storage depths with HVO collaborators showing that crystals, and thus magma, likely came from the shallower HMM reservoir of Kīlauea (Fig. 1a and b). It is worthwhile to note that the number of fluid inclusions reported on day 1 (N = 16) is comparable with many melt inclusion (MI) studies, which often aim for ~20 per sample but frequently report fewer. For example, Lerner *et al.* (2021) reported only 9 MI from the 2018 eruption with sufficient data to calculate saturation pressures (counting MI with glass major-element contents and $H_2O$ contents, MI with glass $CO_2$ measurements if there was no bubble, and glass + bubble measurements if a bubble was present). Using the same criteria, Aster *et al.* (2016) only reported 13 measurements from Lassen Peak, California.

We also had an additional ~20 fluid inclusions fully prepared and catalogued for Raman analysis by the end of day 1. On day 2, these 20 fluid inclusions were analyzed, while additional fluid inclusions were prepared and catalogued for analysis on the following day. After analysis of ~15 crystals, we removed them from CrystalBond™* and placed them on tape for epoxy mount-making. Epoxy was poured at the end of day 2. By ~8:30 pm PST on day 2, we shared an updated histogram of 46 fluid inclusion pressures and depths from 28 crystals, confirming the dominant contribution of the HMM reservoir (Fig. 1a and c). On day 3, we finished analyzing the remaining prepared fluid inclusions. Then, we polished the epoxy mount and catalogued the crystal regions closest to each fluid inclusion to perform EDS analyses. On day 4, Fo contents were determined by EDS, providing a framework to further interpret the plumbing system (Fig. 1d). The Fo content of an olivine is a function of MgO and FeO in the liquid and the Ol-Liq partitioning coefficient ($K_D$). Thus, the Fo contents of the host olivine close to each fluid inclusion can be used to assess the calculated storage depth in its broader petrographic context (e.g. distinguishing high-Fo-olivines that crystallize from more primitive melts from low Fo-olivines forming in more evolved melts). This olivine Fo content was also used to estimate the likely entrapment temperature of each fluid inclusion (DeVitre & Wieser, 2024), and update fluid inclusion pressures from those calculated on days 1–2 using a uniform temperature estimate.

Our results on day 4 clearly show that the majority of fluid inclusions were entrapped at ~1–2 km below the surface (Fig. 1d), which aligns well with depths of the HMM reservoir interpreted using geophysical techniques (Baker & Amelung, 2012; Anderson & Poland, 2016; Anderson *et al.*, 2019), melt inclusion barometry (Lerner *et al.*, 2021; Wieser *et al.*, 2021) and fluid inclusions (DeVitre & Wieser, 2024; Lerner *et al.*, 2024). While the greater number of

analyses from data processed on days 2 and 4 certainly enhance the story, it is notable that depths calculated on day 1 fall within the final proposed storage reservoir depths. Rapid EDS analyses of Fo contents close to each fluid inclusion reveals that olivine crystals grew from a wide range of melt compositions. It is interesting to note that fluid inclusions in the cores of high-Fo- (e.g. >86) olivine crystals return pressures indicative of the shallower HMM reservoir: it has been suggested based on previous eruptions, that these high-Fo crystals predominantly grow in the deeper south caldera reservoir (Fig. 1a) where high-MgO melts are thought to reside (Helz *et al.*, 2014; Pietruszka *et al.*, 2015, 2018; Wieser *et al.*, 2019; Lerner *et al.*, 2024). We suggest three possible scenarios to explain the relatively shallow pressures documented in high-Fo crystals:

1) Fluid inclusions in high-Fo crystals were entrapped within the south caldera reservoir and then transported into the HMM reservoir, where fluid inclusions re-equilibrated to lower pressures prior to eruption over shorter timescales than would be required to reset the host Fo content.

2) High-MgO melts were injected into the HMM reservoir, where high-Fo olivine crystallized and trapped fluid inclusions at shallow depths (Lerner *et al.*, 2024).

3) Complex skeletal growth of olivine crystals during extensive undercooling (Welsch *et al.*, 2013) could mean that high-Fo cores, which initially grew in the south caldera reservoir texturally evolved and trapped lower pressure fluid inclusions in the HMM reservoir.

We think that scenario 1 is unlikely given that fluid inclusions from the 2018 lower East River Zone eruption show no evidence in their densities having been re-equilibrated, despite stalling in the HMM reservoir for up to 2 years (Mourey *et al.*, 2023). Fluid inclusion re-equilibration models of this scenario also indicate <10% change in pressure is expected under these conditions (DeVitre & Wieser, 2024). Current data do not allow us to resolve scenario 2 versus 3, but this eruption could provide an opportunity to explore this further, such as through detailed phosphorous mapping in olivine around fluid inclusions (similar methods were applied to melt inclusions by Esposito *et al.*, 2023). Regardless of the exact mechanism, our fluid inclusion pressures indicate that erupted crystal cargo experienced storage at HMM reservoir depths prior to eruption, and thus this was probably the reservoir supplying magma to the surface during the September 2023 eruption.

## Advantages and limitations of fluid inclusion barometry

Fluid inclusion barometry, using either micro-thermometry or Raman spectroscopy requires very little sample preparation, analytical time and data processing, allowing for a fast turn-around from sample to magma storage pressures and depths. In the case of Raman spectroscopy, a single polished crystal, with a fluid inclusion within ~50 μm of the surface is sufficient to perform high-quality analyses. For micro-thermometry, a doubly polished crystal or slab is needed. Data obtained from either method can quickly be converted into magma storage pressures and depths using an estimated entrapment temperature and an EOS. Recent software developments also allow for more streamlined and reproduceable data-processing routines for analysis of $CO_2$(+$H_2O$) fluids, which means that hundreds of Raman spectra and/or homogenization temperatures can be converted to magma storage pressures and depths within minutes (Wieser & DeVitre, 2024).

One major advantage of fluid inclusion barometry is that the conversion of $CO_2$ density to pressure is relatively insensitive to the choice of entrapment temperature, a parameter, which may not be known at the onset of a new eruptive episode (Fig. 2a–b). The maximum difference in pressure for EOS calculations performed at the lower and upper limit of liquidus temperatures for olivine-saturated melts erupted at Kīlauea throughout its history (~1100 and 1350 °C; DeVitre & Wieser, 2024) is ~20%, which corresponds to an error of about ±0.1–0.2 km at depths representative of the HMM reservoir (1–2 km), and approximately ±0.3–0.5 km at the depths of the south caldera reservoir (3–5 km; Fig. 2b and Figs S3–S6). These errors are of similar magnitude to those associated with the conversion of pressures to depths using an estimate of crustal density (an issue affecting all petrological barometers).

There are a few important limitations of the fluid inclusion method that should be considered, particularly if the goal is to implement it as a near-real-time monitoring tool during an eruptive event. First, it requires the presence of exsolved near-pure $CO_2$ fluids trapped in crystals, whether they are phenocrysts, antecrysts and/or xenocrysts entrained by an erupted magma. Erupted xenoliths have traditionally been a prime target for fluid inclusion barometry as they often contain large numbers of secondary fluid inclusions trapped by fracturing and annealing of crystals under the presence of $CO_2$-rich fluids in the wall rocks of magmatic reservoirs (Roedder, 1965, 1984; Andersen & Neumann, 2001; Hansteen & Klügel, 2008). Although fluid inclusions are not uncommon in phenocrysts and antecrysts, they can be less frequent than melt inclusions, but this is very sample dependent. For example, in our sample suite, we found approximately one in ten crystals hosted fluid inclusions. In $CO_2$-undersaturated systems, fluid inclusions will be absent, but they may be sparse in systems with a low volume fraction of exsolved volatiles (e.g. just saturated).

In principle, fluid inclusions reflect the conditions at the time of entrapment if they satisfy what are commonly known as 'Roedder's rules' (Roedder, 1984). At the time of entrapment, a single homogenous fluid phase must have been trapped (e.g. pure vapor/liquid $CO_2$), and after entrapment, the fluid inclusion must have retained its volume, and nothing must be added or removed (Roedder, 1984; Hansteen & Klügel, 2008). Several challenges arise from natural deviations of these rules. First, magmatic fluid inclusions can often trap mixtures of fluids (e.g. $H_2O$, $CO_2$, $SO_2$, $N_2$, CO, $H_2S$, etc.). It is generally accepted that a few mol. % of a different fluid does not have significant effects on fluid inclusion barometry, but it can contribute to increased uncertainty (Fig. 2c and d; Hansteen & Klügel, 2008). For example, it is not uncommon for $H_2O$ to be present in exsolved magmatic fluids trapped in fluid inclusions, making the use of a mixed $H_2O$–$CO_2$ EOS necessary to calculate pressure from $CO_2$ density. This requires estimating the mol. % $H_2O$ in the inclusion at the time of entrapment, which is often not straightforward as $H_2O$ can be lost via diffusion through the host crystal (Sterner & Bodnar, 1989; Bakker & Jansen, 1991; Mavrogenes & Bodnar, 1994; Frezzotti *et al.*, 2012) or reacted with the host crystal forming carbonate and/or talc (Frezzotti *et al.*, 2012; Sendula *et al.*, 2021). When $H_2O$ has not been lost, the mol. % $H_2O$ in the fluid inclusion can sometimes be measured by Raman spectroscopy if the fluid inclusion is heated to >150 °C (Berkesi *et al.*, 2012) where $H_2O$ and $CO_2$ are miscible. In many cases, studies have often simply assumed that $H_2O$ has been lost, and corrected the measured density based on the molar proportion of $H_2O$ (i.e. $X_{H_2O}$ ~10 mol. %; Klügel *et al.*, 2005; Hansteen & Klügel, 2008; Hildner *et al.*, 2011, 2012). From there, pressures can be calculated using a mixed $H_2O$–$CO_2$ EOS. In general, <10 mol. % $H_2O$ in the fluid causes a relatively

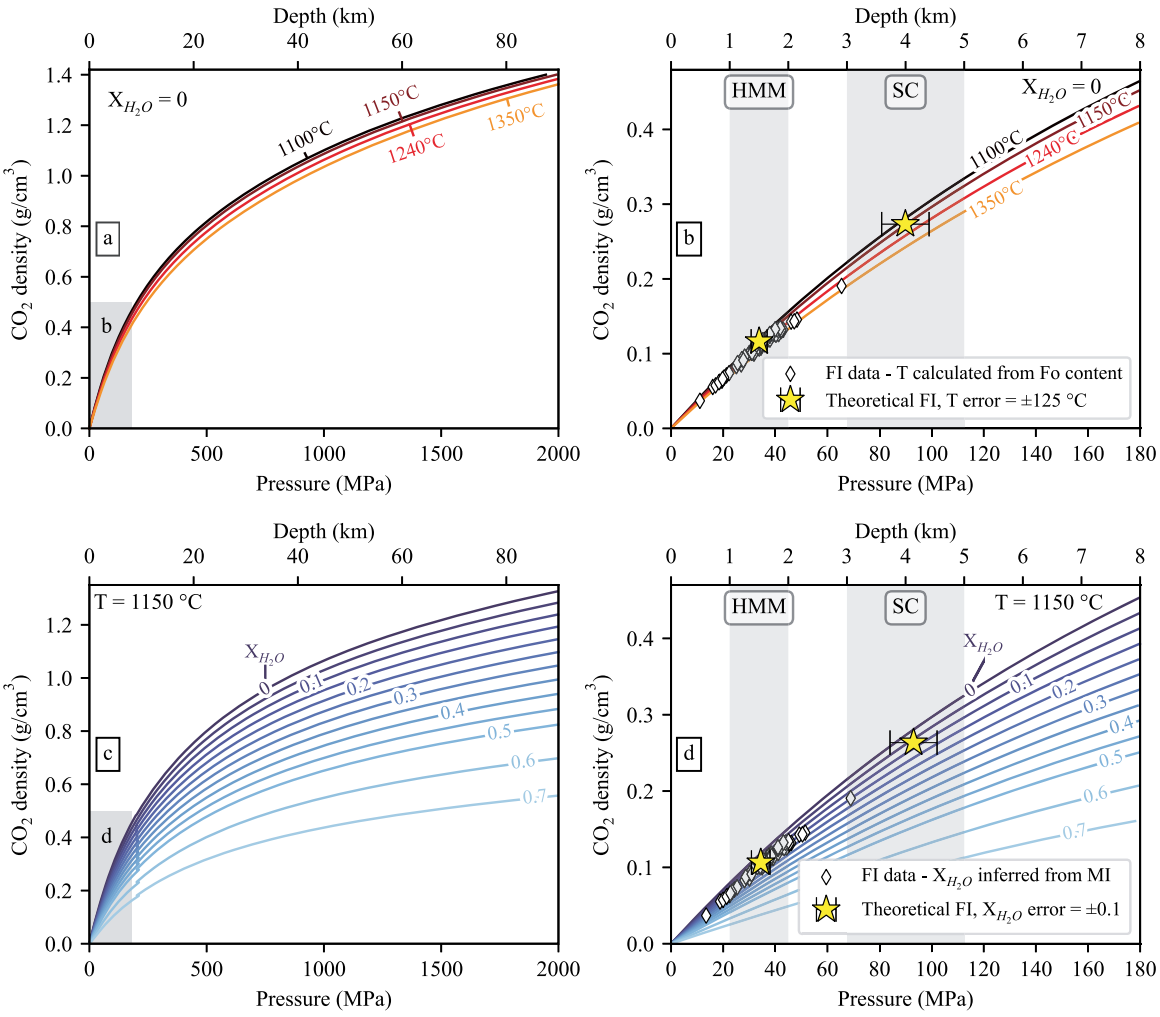


**Fig. 2.** Sensitivity of fluid inclusion barometry to temperature and molar proportions of $H_2O$ in the exsolved fluid phase ($X_{H_2O}$). (a) $CO_2$ density versus pressure for different magmatically relevant entrapment temperatures at Kīlauea using the pure $CO_2$ EOS of Span & Wagner (1996). Temperatures of 1100 and 1350 °C are the lower and upper limit of the liquidus for olivine-saturated melts erupted at Kīlauea throughout its history, and 1150 °C was the temperature used for calculations during days 1 and 2 of the simulation, with 1240 °C being the rounded mean and median of all measured temperatures used for our final dataset. (b) Close-up of panel a. Gray boxes show Kīlauea magma storage inferred from fluid inclusions, melt inclusions and geophysical interpretations (DeVitre & Wieser, 2024; Lerner *et al.*, 2024). HMM = Halema'uma'u reservoir, SC = south caldera reservoir. Stars show hypothetical fluid inclusions trapped at Halema'uma'u and south caldera pressures/depths with $T = 1150$ °C and error-bars representing 1σ uncertainty from Monte Carlo simulations using a temperature uncertainty of ±125 °C ($\frac{1350^\circ C - 1100^\circ C}{2}$). (c) Density of $CO_2$ versus pressure at 1150 °C for various $X_{H_2O}$ using the mixed $H_2O$–$CO_2$ EOS of Duan & Zhang (2006). The small discontinuity at 200 MPa is due to parameter values being switched (see Yoshimura, 2023). (d) Close-up of panel c. Stars show hypothetical fluid inclusions trapped at Halema'uma'u and south caldera with $T = 1150$ °C, $X_{H_2O}$ inferred using the $X_{H_2O}$ -*P* relationship of DeVitre & Wieser (2024). Error bars represent 1σ uncertainty from Monte Carlo simulations using an $X_{H_2O}$ uncertainty of ±0.1 based on the maximum range of $X_{H_2O}$ inferred in our dataset ($\frac{XH_2Omax - XH_2Omin}{2}$) when calculated using the upper limit$X_{H_2O}$-P relationship for Kīlauea from DeVitre & Wieser, 2024.

small difference in calculated pressures and depths, though the effect is more pronounced at higher $CO_2$ densities (Fig. 2c and d). For instance, with a $X_{H_2O} = 10$ mol. %, the difference in pressure between pure $CO_2$ (Span & Wagner, 1996) and mixed $H_2O$–$CO_2$ (Duan & Zhang, 2006) EOS is only ~10% at 30 MPa (~1 km) and ~17% at 800 MPa (~35 km; Fig. 2c and d). Higher mol. % $H_2O$ in the fluid can be expected in certain shallow, water-rich volcanic systems (such as those in subduction zones), which would result in a much more significant error if $X_{H_2O}$ is not constrained and/or too high. This raises the importance of assessing the composition of fluid inclusions and constraining, at least approximately, $X_{H_2O}$ in the fluid. Fluid inclusion barometry will only be applicable using near-pure $CO_2$ inclusions.

As mentioned previously, to reflect entrapment conditions fluid inclusions must also have retained their volume and nothing must be added or removed after entrapment. This gives rise to another complication: After entrapment, and as the host crystal ascends in the magma plumbing system, strong pressure gradients will arise between the exterior of the crystals and the entrapped fluid inclusions. Large pressure gradients result in volumetric re-equilibration of the fluid inclusions either by plastic deformation of the host crystal (commonly referred to as stretching) or brittle deformation (termed decrepitation) (Kirby & Green, 1980; Wanamaker & Evans, 1989; Viti & Frezzotti, 2000; Yamamoto *et al.*, 2002, 2007, 2011; Bodnar, 2003; Hansteen & Klügel, 2008). This means that fluid inclusions will generally reflect minimum entrapment pressures, particularly when they were originally entrapped at high pressure (>10 km depth). The higher the internal pressure of the fluid inclusion, the faster the re-equilibration will be at various levels of ascent.

In the case of shallow systems like Kīlauea, if inclusions are trapped at <7 km depth, re-equilibration via plastic deformation on timescales relevant to recharge and eruption (months to a decade; Mourey *et al.*, 2023; Lynn *et al.*, 2024b) is generally not of concern as the internal pressure of the inclusions is very low and the predicted change in pressure, even over a decade, is within the uncertainty of the measurements (<10%; DeVitre & Wieser, 2024). In deeper magmatic plumbing systems, such as the Canary Islands, Galápagos Islands or Cabo Verde, significant re-equilibration will likely occur within days and fluid inclusions almost never reflect original entrapment depths. However, because fluid inclusions are so sensitive to re-equilibration, they are excellent recorders of stalling events throughout a magmatic plumbing system, and preferentially record the last stage of storage prior to eruption (Hansteen & Klügel, 2008). This is, in fact, a benefit of rapid response studies, as this final staging zone is likely the most relevant to understand the reservoir supplying the magma to the surface.

From the perspective of choosing suitable samples for fluid inclusion work, it has been suggested that fluid inclusions from crystals in lava flows may re-equilibrate more readily than those in tephras (Klügel *et al.*, 2020), as the former cool slower. As for magma stalling in the crust, the effect of re-equilibration will be more significant for fluid inclusions entrapped at high pressures. In shallower systems, no significant difference is observed between naturally quenched lava flow samples and those rapidly quenched in water (DeVitre & Wieser, 2024), and re-equilibration models do not predict any changes in density outside analytical uncertainty. For a given fluid inclusion density, size and ascent path, it is possible to model the predicted re-equilibration scenario using a plastic deformation model, allowing assessment of the possible influence of equilibration on the measured density (Wanamaker & Evans, 1989; Yamamoto *et al.*, 2007; DeVitre & Wieser, 2024). We suggest that such models are run when evaluating a suite of samples for rapid response barometry. Once the first few densities are obtained by Raman spectroscopy and fluid inclusion sizes measured, models for different re-equilibration scenarios should be considered (e.g. syn-eruptive quenching, crustal stalling) before interpreting and reporting results.

## Broader applicability of the method

The use of a pure $CO_2$ EOS results in an underestimate of entrapment pressures of fluid inclusions if there was $H_2O$ in the fluid at the time of fluid inclusion entrapment (Figs 1 and 2). This is the main factor limiting the global applicability of the fluid inclusion barometry technique. At Kīlauea, melt inclusion data indicate that the exsolved fluid phase is ∼90% $CO_2$ at pressures corresponding to the HMM reservoir, and > 95% $CO_2$ at pressures indicative of the south caldera reservoir (Wieser *et al.*, 2021; DeVitre & Wieser, 2024). This means that the effect of $\mathbf{X}_{H_2O}$ is very small on calculated pressures presented here (Fig. 1d). Given that re-equilibration is not a significant concern on timescales relevant to pre-eruptive storage and syn-eruptive transport at Kīlauea (DeVitre & Wieser, 2024), we can conclude that fluid inclusion barometry is a useful and reliable technique at this volcano.

To assess the utility of the method for rapid-response petrology globally, it is necessary to evaluate the distribution of $\mathbf{X}_{H_2O}$ contents in different tectonic regions, and the effect of this parameter on calculated fluid inclusion pressures. To do this, we compiled published melt inclusion data from all over the world, spanning many different tectonic settings (see supplement for compilation details). We calculate $\mathbf{X}_{H_2O}$ using the solubility model MagmaSat (Ghiorso & Gualda, 2015), implemented in VESIcal (Iacovino *et al.*, 2021) using a custom multiprocessing routine in Python (supplement for details). For each volcano, there is a clear correlation between $\mathbf{X}_{H_2O}$ and pressure, with $\mathbf{X}_{H_2O}$ increasing drastically at shallow pressures (Figs 3 and S8a–i), likely reflecting the entrapment of melt inclusions during ascent (often enhanced by changes in phase stability and liquidus temperature during $H_2O$ degassing; Applegarth *et al.*, 2013). Thus, in this compilation, the median and 25th percentiles are most representative of $\mathbf{X}_{H_2O}$ in the main magma storage region. For this reason, we show the distribution (median, 25th and 75th percentiles) of calculated $\mathbf{X}_{H_2O}$ for 4069 melt inclusions with $SiO_2$ of <57 wt. %, MgO of <16 wt. %, and saturation pressure > 20 MPa on Fig. 4b and c, colored by tectonic setting. We stress the importance of considering the possible range of $\mathbf{X}_{H_2O}$values when determining the suitability of this method to a particular system, and the fact that the $\mathbf{X}_{H_2O}$ pressure correction tends to be more significant at higher entrapment pressures. For example, if we consider a $\mathbf{X}_{H_2O}$ value of 0.1 (the median $\mathbf{X}_{H_2O}$ of our fluid inclusion dataset at Kīlauea and a commonly assumed $\mathbf{X}_{H_2O}$ in deep storage systems), the pressure correction goes from <15% at pressures of <220 MPa (∼10 km) to ∼20% at 700 MPa (∼30 km). This correction is even more significant if $\mathbf{X}_{H_2O}$ is greater than 0.1 (e.g. for $\mathbf{X}_{H_2O} = 0.2$, the correction is 25%–30% at $P < 150$ MPa and ∼50% at $P = 700$ MPa; Fig. 2).

Most melt inclusion suites in our global compilation did not have measurements of $CO_2$ in the vapor bubble, meaning that the total $CO_2$ content has been underestimated and $\mathbf{X}_{H_2O}$ overestimated. This can be demonstrated by comparing $\mathbf{X}_{H_2O}$ values at volcanoes where there are some studies with Raman spectrometry measurements and some without (Fig. S8c East African Rift; Fig. S8h Kamchatka and Cascade arc systems). Figure 4c shows a compilation only using melt inclusions where bubble $CO_2$ was measured by Raman spectroscopy. Both compilations demonstrate that subduction zones record much higher $\mathbf{X}_{H_2O}$ globally than mid-ocean ridge basalts, ocean island basalts, continental rift and intraplate volcanoes. It is also interesting that within hotspot and intraplate settings, regions with tholeiitic compositions (e.g. Iceland, Hawai'i, Galápagos Islands, Réunion, Deccan Traps) generally have lower $\mathbf{X}_{H_2O}$ values than regions with more alkalic magmas (e.g. Canary Islands, Azores, Cabo Verde, Fig. 5). This likely represents the lower degrees of partial melting that produce alkalic magmas, and the possibility of more volatile-rich sources (DeVitre *et al.*, 2023). Overall, this compilation indicates that rapid-response fluid inclusion barometry is highly applicable to active volcanic regions such as Hawai'i, Iceland, the East African Rift, Galápagos Islands, Réunion, Cabo Verde and Canary Islands (Fig. 5). However, it is not appropriate in subduction zones such in Alaska, Kamchatka or Central America, where $\mathbf{X}_{H_2O}$ is very high. Although there are only two studies that use Raman spectroscopy data in the Cascade Range arc system (Aster *et al.*, 2016; Venugopal *et al.*, 2020), and one for the Kamchatka arc system (Moore *et al.*, 2018), in both cases fluid inclusions with highest pressures have $\mathbf{X}_{H_2O}$ values of <0.2. This may indicate that in drier subduction zones, fluid inclusions may have some utility for the most mafic, $CO_2$-rich magmas.

We acknowledge that many systems do not have detailed melt inclusion measurements to accurately calculate $\mathbf{X}_{H_2O}$ (particularly given the paucity of studies worldwide measuring both bubble and glass phases of melt inclusions; Wieser *et al.*, 2024). However, the knowledge of the tectonic setting of a volcano and its phase assemblage, alongside this database, can be used to assess the potential for fluid inclusion barometry. Unless detailed melt

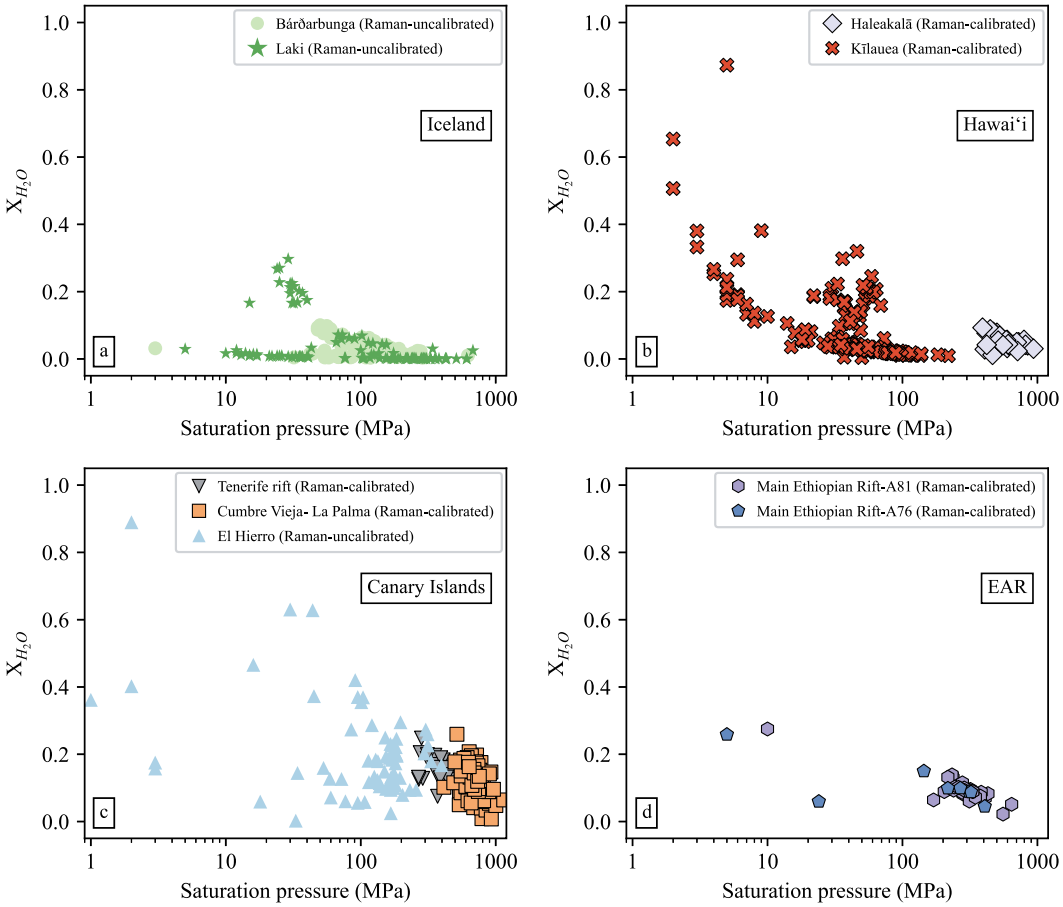


**Fig. 3.** Examples of pressure versus $X_{H_2O}$ for some recently active mafic volcanic systems (a–c) and the East African Rift (d), where fluid inclusion barometry could be used as a near-real-time monitoring tool. Data shown for melt inclusions with reconstructed total $CO_2$ using Raman spectroscopy (see supplementary information for extended details on the compilation). Outlined symbols represent data collected using a Raman spectrometer with an instrument-specific calibration. Filled symbols with no outline are data that did not use an instrument specific calibration. The supplementary information contains similar plots for every location in the compilation, including glass-only melt inclusion volatile data (Fig. S8a–i). Iceland data from (Hartley *et al.*, 2014; Bali *et al.*, 2018), Hawai'i from (Lerner *et al.*, 2021; Moore *et al.*, 2021; Wieser *et al.*, 2021), Canary Islands from (Taracsák *et al.*, 2019; DeVitre *et al.*, 2023; Dayton *et al.*, 2024) and East African Rift from (Wong *et al.*, 2023).

inclusion measurements have been performed to demonstrate high $CO_2$, low $H_2O$ magmas, fluid inclusion barometry is not applicable for near-real-time monitoring of arc volcanoes. However, for an ocean island basalt (OIB) setting with no prior data, after classifying the composition as alkalic or tholeiite, one could perform a correction by fitting a polynomial to the alkalic or tholeiitic OIBs in the global dataset, including a generous error window, which would be propagated through to calculated pressures. As more data become available (e.g. post eruption), these estimates could be revised to better estimate magma storage pressures and depths. For volcanoes that are not currently erupting but have had historical eruptions, an informed guess on a likely $\mathbf{X}_{H_2O}$ range can be made using chemical information from previous eruptive events. For instance, one could easily determine the chemical tendency of a volcano (e.g. alkaline vs tholeiitic) from already existing major-element data (Fig. 5a). In many cases, even when no chemical data are available for a specific volcano, an analog estimate may be drawn from neighboring volcanoes. For example, during the 2022 eruption of Mauna Loa, no detailed melt inclusion measurements (including vapor bubbles) were available. However, as a first estimate, the P-$\mathbf{X}_{H_2O}$ relationships from neighboring Kīlauea could be used. We note that once arc magmas are excluded from the compilation, even if $\mathbf{X}_{H_2O}$ is entirely unconstrained, fluid inclusion barometry is still more accurate than other methods, such as mineral-melt thermobarometry in calculating magma storage pressures.

Looking forward, to increase the accuracy of rapid-response petrological monitoring during future eruptions, performing melt inclusion studies, accounting for vapor bubble $CO_2$ in more volcanic systems worldwide, would greatly improve overall understanding, given the large offsets between studies accounting for bubbles and those which do not in $\mathbf{X}_{H_2O}$ space (Fig. 4), and to determine approximate trends in $\mathbf{X}_{H_2O}$-pressure space for a given volcanic system or region during times of quiescence. This will allow assessment of the suitability of the fluid inclusion method for a given volcano and permit appropriate corrections for the complexities of mixed fluids without requiring melt inclusion work during each eruptive episode. In systems with no prior constraints, our observations of correlations between alkalinity and $\mathbf{X}_{H_2O}$ can provide a first order assessment of appropriate $\mathbf{X}_{H_2O}$ values. Better constraints of $\mathbf{X}_{H_2O}$ is also vital for other petrological workflows, such as calculating phase stabilities, performing experiments, and modeling vapor saturation and eruption triggering.

## Relevance of near-real-time data for observatories

Our simulation demonstrates that rapid-response fluid inclusion barometry can be performed in near-real-time and such

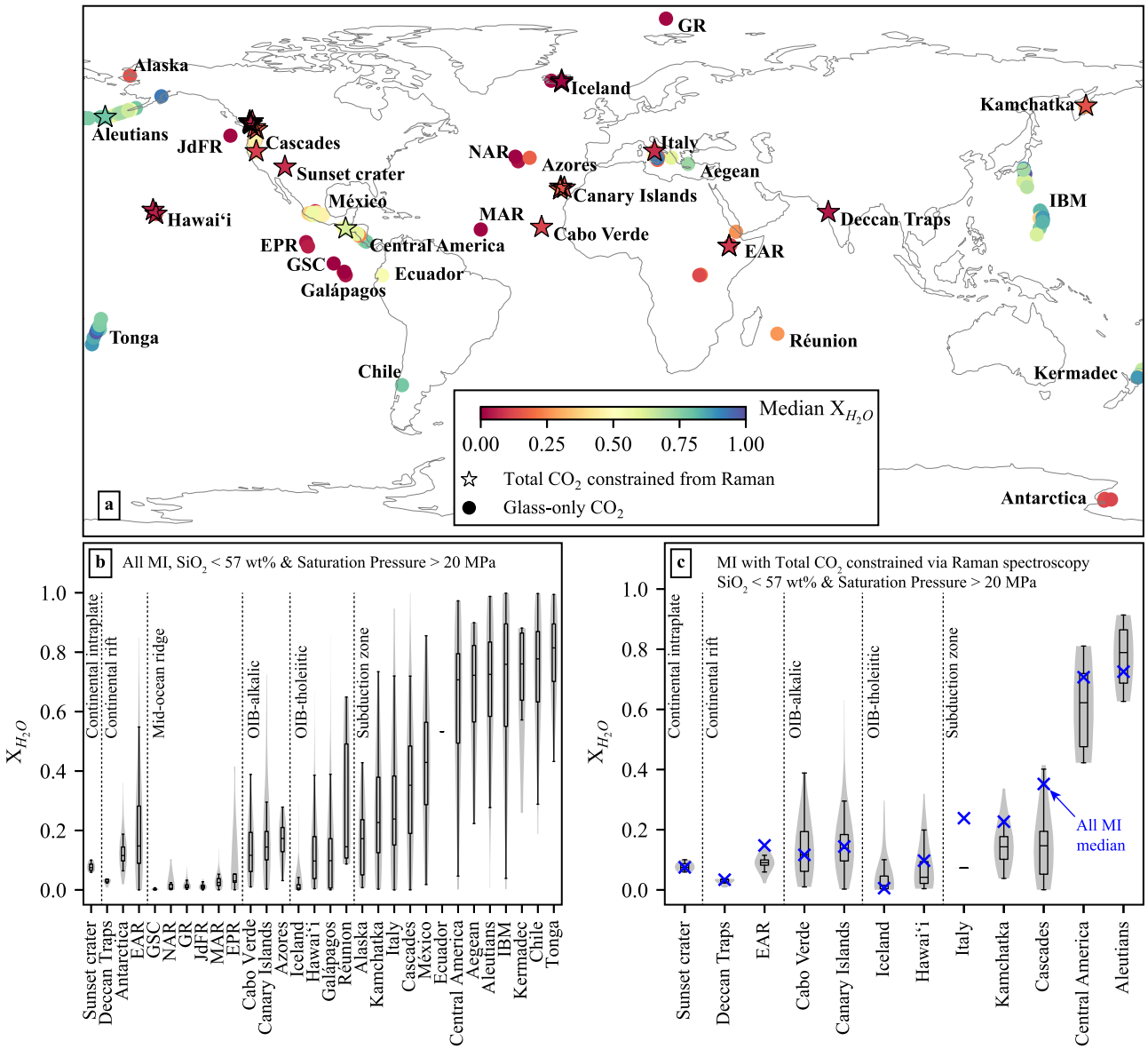


**Fig. 4.** Global compilation of $X_{H_2O}$ in the exsolved fluid phase from melt inclusion data for continental rift, continental intraplate, alkalic and tholeiitic ocean island basalt (OIB, see Fig. S7), mid-ocean ridge and subduction zone volcanoes (details and references in the supplementary information) (a) World map with symbols colored by median $X_{H_2O}$ of the melt inclusion suites. Circles indicate glass-only melt inclusion data and stars show those for which $CO_2$ has been constrained by Raman spectroscopy. (b) Boxplot of $X_{H_2O}$ for melt inclusion suites plotted on panel a. Boxplots show the median, Q1 (25th percentile), Q3 (75th percentile), and whiskers mark the last data point before Q3 + 1.5* (Q3-Q1) and the first data point after Q1 – 1.5*(Q3-Q1). Violin plots show the density distribution of all data. (c) Boxplot of $X_{H_2O}$ showing only melt inclusion suites with constrained total $CO_2$ by Raman spectroscopy. EAR—East African Rift, GSC—Galápagos Spreading Center, NAR—North Atlantic Ridge, JdFR—Juan de Fuca Ridge, GR—Gakkel Ridge, MAR—Mid-Atlantic Ridge, EPR—East Pacific Rise, IBM—Izu-Bonin Mariana. Data are filtered to $SiO_2$ of <57 wt. %, MgO of <16 wt. %, and saturation pressure > 20 MPa (see supplementary information for details). Crosses indicate median $X_{H_2O}$ calculated considering all melt inclusions (with and without Raman spectroscopy measurements).

rapid-response work in collaboration with universities was not taxing on observatory or academic staff. In future eruptions at poorly characterized systems, this method could be used to help observatories deduce the geometry of the plumbing system supplying magma to the surface. In well-characterized systems such as Kīlauea, where the location of different reservoirs have been identified by prior petrological and geophysical studies, this method can be used to determine which reservoir (or combination of reservoirs) is supplying the eruption, without detracting from other essential duties during eruption responses. For example, during the 2018 lower East Rift Zone eruption of Kīlauea, HVO's near-real-time chemical monitoring of bulk-rock samples via energy dispersive X-ray fluorescence (ED-XRF) identified multiple magma compositions (Gansecki *et al.*, 2019). Fluid inclusion barometry could have linked these distinct chemical signatures to different storage regions, addressing the questions of scientists and residents alike. Indeed, in active volcanic regions (especially in places like Hawai'i), both the scientific community and the local residents commonly want to know where magma is coming from. Sharing scientific results and information is an integral part of the mission of volcanic observatories. In the United States, for example, volcano observatories have the mandate to make such information and data available to the public under the 'USGS Public Access Plan'

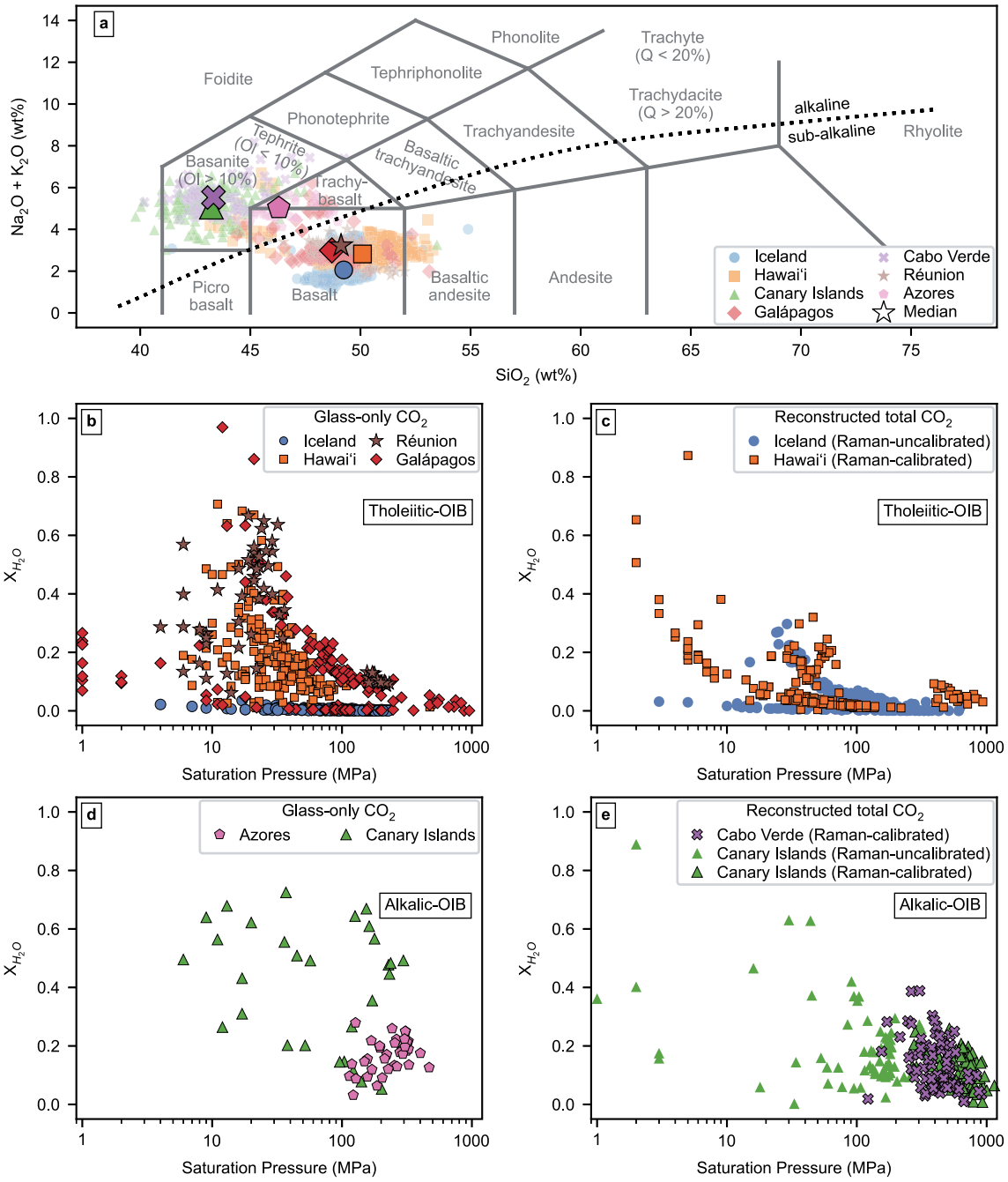


**Fig. 5.** Pressure versus $X_{H_2O}$ for tholeiitic and alkalic ocean island volcanoes. (a) Total alkali versus silica diagram (Le Maitre *et al.*, 2002) plotted using python tool tasplot available on BitBucket (https://bitbucket.org/jsteven5/tasplot/src/master/) and PyPI. The alkalic versus sub-alkalic trend is adapted from Miyashiro (1974). (b–c) Pressure versus $X_{H_2O}$ for tholeiitic ocean island volcanoes, (b) panel shows melt inclusions with $CO_2$ constrained only in the glass phase and (c) panel shows melt inclusions with reconstructed total $CO_2$ using the glass phase $CO_2$ and $CO_2$ in the vapor bubble measured via Raman spectroscopy. On panel c, symbols with an outline indicate that $CO_2$ density from Raman spectroscopy was calculated using an instrument specific calibration while symbols with no outline were calculated without. (d–e) Panel shows the same as panels b–c but for alkalic ocean island volcanoes.

(https://www.usgs.gov/office-of-science-quality-and-integrity/fundamental-science-practices/public-access-results-federally-funded-research-us).

The return of eruptive activity to the summit of Kīlauea in December 2020 was accompanied by many questions about how the magmatic plumbing system had changed following >500 m of summit caldera collapse in 2018 (Lynn *et al.*, 2024b). At the time, it was uncertain whether renewed activity could bring the return of lava lake, shallow-sourced eruptions or perhaps a new East Rift Zone eruption. Near-real-time fluid inclusion barometry could have helped understand the state of the magmatic plumbing system and show that despite the summit collapse, the HMM reservoir was still primed to support shallow eruptions as it had in years past. In contrast with Kīlauea, very little information about Mauna Loa's plumbing system was available when it erupted in 2022 (Lynn *et al.*, 2024c). In such a case, near-real-time fluid inclusion barometry could have provided a quick snapshot and been very

useful to help understand Mauna Loa's poorly characterized system.

Fluid inclusion barometric data could also aid in understanding reservoirs being tapped during a long-lived eruption and supplement syn-eruptive deformation and stress changes, which are measured in real time by geophysical methods (i.e. tilt, GPS, seismic and gravity). Fluid inclusions in erupted crystals are the only concrete way in which geophysical and/or conceptual models can be validated or challenged given that no other petrological method can access depth information in near-real time. Ultimately, having a long timeline of fluid inclusion barometric data increases an observatory's forecasting abilities when leveraging this additional data along with monitoring data.

The case study presented here intentionally targeted a low-hazard eruption as a test for implementing near-real-time fluid inclusion barometry as a monitoring tool. This type of work, on low-hazard, short-lived eruptions, has a few advantages. First, it allows observatories and their partners to work out bottlenecks to implement the tool for future events. Second, it enables researchers to establish baselines that can be used for routine monitoring, which is fundamental to notice changes and trends in volcanoes like Kīlauea, which have frequent eruptive activity and evolve over human timescales (Swanson *et al.*, 2014). Although the September 2023 eruption was short lived, one can also imagine how such data could be useful in the context of a much longer eruption (e.g. Kīlauea's 2018 lower East Rift Zone). For instance, if fluid inclusion barometry indicated depths of ≥5 km, these data could hypothetically be used to inform discussions about the potential for a deeper source than seen in previous events, and therefore an expectation for possible greater volume, increased duration or potential waxing and waning if magma transport involves shallow sources along the way. We envision that other observatories worldwide (e.g. in Cabo Verde, Galápagos Islands, Canary Islands, Iceland, etc.) could include fluid inclusion barometric data as part of their monitoring routines either in-house or through partnerships with academic institutions.

## CONCLUSIONS

Our simulation shows that magma storage pressures and depths can be determined within a day of receiving samples, with modest resources and personnel requirements (e.g. no overnight shift work, with normal semester teaching and class schedules). For example, sample preparation was carried out using transmitted-reflected light microscopes from the UC Berkeley's teaching collection, using only a research-grade microscope for sample cataloging. Raman spectrometers are widely available at many universities, given that it is a popular technique used in many fields of study, such as material sciences, physics, chemistry and biology, and the W-filament SEM used for EDS analyses to measure olivine Fo contents has been around for 15 years (S1 Appendix).

This work demonstrates the importance of rapid-response work in collaboration with universities in not being taxing on observatory or academic staff, particularly considering the usefulness of information provided. This means the methodology can be employed during future eruptions to help observatories estimate the geometry of the plumbing system supplying magma, adding crucial information (Re *et al.*, 2021), without detracting from other essential duties during eruption responses.

Our global compilation of $\mathbf{X}_{H_2O}$ values shows that fluid inclusion barometry has utility as a rapid-response petrological monitoring method at many of the world's most active and hazardous basaltic volcanoes (e.g. Hawai'i, Galápagos Islands, Réunion, Azores, Canary Islands, Iceland, Cabo Verde and the East Africa Rift). As our understanding of exsolved fluid compositions improves and more studies account for $CO_2$ held within vapor bubbles, it is likely that the applicability of the rapid-response fluid inclusion barometry method may expand to even more volcanic systems (e.g. drier arc magmas such as in the Cascade Range or Kamchatka).

Overall, fluid inclusion barometry is broadly applicable and adds valuable quantitative storage depth information that provides a key advancement for volcano observatories that utilize near-real-time geochemical monitoring to better understand eruptions as they unfold (see overview–(Re *et al.*, 2021); Hawai'i–(Gansecki *et al.*, 2019); La Palma–(Pankhurst *et al.*, 2022); Fuego–(Liu *et al.*, 2020); Italy–(Corsaro & Miraglia, 2022)).

## SUPPLEMENTARY DATA

Supplementary data are available at *Journal of Petrology* online.

## ACKNOWLEDGEMENTS

Any use of trade, product or firm names is for descriptive purposes only and does not imply endorsement by the US Government.

## FUNDING

The study is supported by National Science Foundation (grant no. EAR 2217371 to PW, CLD, BR, AR), and the Berkeley Rose Hills Innovator Program (PW and CLD).

## AUTHOR CONTRIBUTIONS

Author contributions for lab work are shown on Fig. S1. CD and PW wrote the paper. CD, PW, AR, BR and AB prepared tephra, picked olivine, found fluid inclusions, cataloged and mounted them, and conducted Raman analyses. CD and PW performed all spectral fitting, data processing and figure making, with schematic cartoons shown in Fig. S1 from AB. JG developed the Mg/Fe calibration for the EDS detector and MG performed EDS analyses with help from JG. KJL, DTD, NID and KMM collected samples, processed them at HVO (in Hilo, Hawai'i), provided eruption context and edited the manuscript.

## CONFLICT OF INTEREST STATEMENT

Authors declare that they have no competing interests.

## DATA AVAILABILITY

All data are made available in the Supplementary Information associated with the publication. We include detailed materials and methods (S1 Appendix), complete processed fluid inclusion dataset (S2 Dataset), the global melt inclusions dataset (S3 Dataset) and a compilation of microphotographs of the fluid inclusions and crystals that were used for navigation only during the simulation (S4 FI Image Compilation). All raw data and Jupyter notebooks are stored on Github at the following link: https://github.com/cljdevitre/RapidresponseFI_Kilauea_Sept2023. The Github repository is archived at Zenodo (https://doi.org/10.5281/zenodo.14194797).

## REFERENCES


Andersen, T. & Neumann, E. R. (2001). Fluid inclusions in mantle xenoliths. *Lithos* **55**, 301–320. https://doi.org/10.1016/S0024-4937(00)00049-9.

Andersen, T., Burke, E. A. J. & Neumann, E.-R. (1995). Nitrogen-rich fluid in the upper mantle: fluid inclusions in spinel dunite from Lanzarote, Canary Islands. *Contributions to Mineralogy and Petrology* **120**, 20–28. https://doi.org/10.1007/BF00311005.

Anderson, K. R. & Poland, M. P. (2016). Bayesian estimation of magma supply, storage, and eruption rates using a multiphysical volcano model: Kīlauea volcano, 2000–2012. *Earth and Planetary Science Letters* **447**, 161–171. https://doi.org/10.1016/j.epsl.2016.04.029.

Anderson, K. R., Johanson, I. A., Patrick, M. R., Gu, M., Segall, P., Poland, M. P., Montgomery-Brown, E. K. & Miklius, A. (2019). Magma reservoir failure and the onset of caldera collapse at Kīlauea volcano in 2018. *American Association for the Advancement of Science* **366**, eaaz1822. https://doi.org/10.1126/science.aaz1822.

Andrews, B. J., Befus, K. S., Blatter, D. L., Coombs, M. L., deGraffenried, R., Hammer, J. E., Gardner, J. E., Larsen, J. F., Shea, T., & Wright, H. M. N. (2019). Rapid experimental determination of magmatic phase equilibria: Coordinating a volcanic crisis response protocol. 2019, V33A-03. AGU Fall Meeting Abstracts.

Applegarth, L. J., Tuffen, H., James, M. R., Pinkerton, H. & Cashman, K. V. (2013). Direct observations of degassing-induced crystallization in basalts. *Geology* **41**, 243–246. https://doi.org/10.1130/G33641.1.

Aster, E. M., Wallace, P. J., Moore, L. R., Watkins, J., Gazel, E. & Bodnar, R. J. (2016). Reconstructing CO2 concentrations in basaltic melt inclusions using Raman analysis of vapor bubbles. *Journal of Volcanology and Geothermal Research* **323**, 148–162. https://doi.org/10.1016/j.jvolgeores.2016.04.028.

Baker, S. & Amelung, F. (2012). Top-down inflation and deflation at the summit of Kīlauea volcano, Hawai'i observed with InSAR. *Journal of Geophysical Research: Solid Earth* **117 (B12)**. https://doi.org/10.1029/2011JB009123.

Bakker, R. J. (2021). The perfection of Raman spectroscopic gas densimeters. *Journal of Raman Spectroscopy* **52**, 1923–1948. https://doi.org/10.1002/jrs.6245.

Bakker, R. J. & Jansen, J. B. H. (1991). Experimental post-entrapment water loss from synthetic CO2-H2O inclusions in natural quartz. *Geochimica et Cosmochimica Acta* **55**, 2215–2230. https://doi.org/10.1016/0016-7037(91)90098-P.

Bali, E., Zajacz, Z., Kovács, I., Szabó, C. S., Halter, W., Vaselli, O., Török, K. & Bodnar, R. J. (2008). A quartz-bearing orthopyroxene-rich Websterite xenolith from the Pannonian Basin, Western Hungary: evidence for release of quartz-saturated melts from a subducted slab. *Journal of Petrology* **49**, 421–439. https://doi.org/10.1093/petrology/egm086.

Bali, E., Hartley, M. E., Halldórsson, S. A., Gudfinnsson, G. H. & Jakobsson, S. (2018). Melt inclusion constraints on volatile systematics and degassing history of the 2014–2015 Holuhraun eruption, Iceland. *Contributions to Mineralogy and Petrology* **173**, 9. https://doi.org/10.1007/s00410-017-1434-1.

Belkin, H. E., de Vivo, B., Roedder, E. & Cortini, M. (1985). Fluid inclusion geobarometry from ejected Mt. Somma-Vesuvius nodules. *American Mineralogist* **70**, 288–303.

Berkesi, M., Guzmics, T., Szabó, C., Dubessy, J., Bodnar, R. J., Hidas, K. & Ratter, K. (2012). The role of CO2-rich fluids in trace element transport and metasomatism in the lithospheric mantle beneath the central Pannonian Basin, Hungary, based on fluid inclusions in mantle xenoliths. *Earth and Planetary Science Letters* **331-332**, 8–20. https://doi.org/10.1016/j.epsl.2012.03.012.

Bodnar, R. J. (2003) Reequilibration of fluid inclusions. In: Samson I., Anderson A. & Marshall D. (eds) *Fluid Inclusions: Analysis and Interpretation*. Mineralogical Association of Canada, Québec City, Quebec, Canada.

Boudoire, G., Pasdeloup, G., Schiavi, F., Cluzel, N., Rafflin, V., Grassa, F., Giuffrida, G., Liuzzo, M., Harris, A., Laporte, D. & Rizzo, A. L. (2023). Magma storage and degassing beneath the youngest volcanoes of the massif central (France): lessons for the monitoring of a dormant volcanic province. *Chemical Geology* **634**, 121603. https://doi.org/10.1016/j.chemgeo.2023.121603.

Clocchiatti, R., Del Moro, A., Gioncada, A., Joron, J. L., Mosbah, M., Pinarelli, L. & Sbrana, A. (1994). Assessment of a shallow magmatic system: the 1888–90 eruption, Vulcano Island, Italy. *Bulletin of Volcanology* **56**, 466–486. https://doi.org/10.1007/BF00302828.

Cooper, K. M., Anderson, K., Cashman, K., Coombs, M., Dietterich, H., Fischer, T., Houghton, B., Johanson, I., Lynn, K. J., Manga, M. & Wauthier, C. (2023). Coordinating science during an eruption: lessons from the 2020–2021 Kīlauea volcanic eruption. *Bulletin of Volcanology* **85**, 29. https://doi.org/10.1007/s00445-023-01644-1.

Corsaro, R. A. & Miraglia, L. (2022). Near real-time petrologic monitoring on volcanic glass to infer magmatic processes during the February–April 2021 paroxysms of the south-east crater, Etna. *Frontiers in Earth Science* **10**. https://doi.org/10.3389/feart.2022.828026.

Dayton, K., Gazel, E., Wieser, P., Troll, V. R., Carracedo, J. C., la Madrid, H., Roman, D. C., Ward, J., Aulinas, M., Geiger, H., Deegan, F. M., Gisbert, G. & Perez-Torrado, F. J. (2023). Deep magma storage during the 2021 La Palma eruption. *Science (New York, NY : Online)* **9**, eade7641. https://doi.org/10.1126/sciadv.ade7641.

Dayton, K., Gazel, E., Wieser, P. E., Troll, V. R., Carracedo, J. C., Aulinas, M. & Perez-Torrado, F. J. (2024). Magmatic storage and volatile fluxes of the 2021 La Palma eruption. *Geochemistry, Geophysics, Geosystems* **25**, e2024GC011491. https://doi.org/10.1029/2024GC011491.

DeVitre, C. L. & Wieser, P. E. (2024). Reliability of Raman analyses of CO2-rich fluid inclusions as a geobarometer at Kīlauea. *Geochemical Perspectives Letters* **29**, 1–8. https://doi.org/10.7185/geochemlet.2404.

DeVitre, C. L., Allison, C. M. & Gazel, E. (2021). A high-precision CO2 densimeter for Raman spectroscopy using a fluid density calibration apparatus. *Chemical Geology* **584**, 120522. https://doi.org/10.1016/j.chemgeo.2021.120522.

DeVitre, C. L., Gazel, E., Ramalho, R. S., Venugopal, S., Steele-MacInnis, M., Hua, J., Allison, C. M., Moore, L. R., Carracedo, J. C. & Monteleone, B. (2023). Oceanic intraplate explosive eruptions fed directly from the mantle. *Proceedings of the National Academy of Sciences* **120**, e2302093120. https://doi.org/10.1073/pnas.2302093120.

Dietterich, H. R. & Neal, C. A. (2022). A look ahead to the next decade at US volcano observatories. *Bulletin of Volcanology* **84**, 63. https://doi.org/10.1007/s00445-022-01567-3.

Duan, Z. & Zhang, Z. (2006). Equation of state of the H2O, CO2, and H2O–CO2 systems up to 10 GPa and 2573.15K: molecular dynamics simulations with ab initio potential surface. *Geochimica et Cosmochimica Acta* **70**, 2311–2324. https://doi.org/10.1016/j.gca.2006.02.009.

Esposito, R., Badescu, K., Boyce, J. W. & Frezzotti, M.-L. (2023). Chemical characterization of a magma recharging and mixing before an eruption: insights from chronologically constrained melt inclusions. *Lithos* **456-457**, 107301. https://doi.org/10.1016/j.lithos.2023.107301.

Fall, A., Tattitch, B. & Bodnar, R. J. (2011). Combined microthermometric and Raman spectroscopic technique to determine the salinity of H2O–CO2–NaCl fluid inclusions based on clathrate

melting. *Geochimica et Cosmochimica Acta* **75**, 951–964. https://doi.org/10.1016/j.gca.2010.11.021.

Frezzotti, M. L., Peccerillo, A. & Bonelli, R. (2003) Magma ascent rates and depths of crustal magma reservoirs beneath the Aeolian volcanic Arc (Italy): Inferences from fluid and melt inclusions in xenoliths. In: De Vivo B. & Bodnar R. J. (eds) *Melt Inclusions in Volcanic Systems - Methods, Applications and Problems*. Elsevier, Amsterdam, Netherlands, pp.185–205.

Frezzotti, M. L., Ferrando, S., Tecce, F. & Castelli, D. (2012). Water content and nature of solutes in shallow-mantle fluids from fluid inclusions. *Earth and Planetary Science Letters* **351-352**, 70–83. https://doi.org/10.1016/j.epsl.2012.07.023.

Gansecki, C., Lee, R. L., Shea, T., Lundblad, S. P., Hon, K. & Parcheta, C. (2019). The tangled tale of Kīlauea's 2018 eruption as told by geochemical monitoring. *American Association for the Advancement of Science* **366**, eaaz0147. https://doi.org/10.1126/science.aaz0147.

Ghiorso, M. S. & Gualda, G. A. R. (2015). An H2O–CO2 mixed fluid saturation model compatible with rhyolite-MELTS. *Contributions to Mineralogy and Petrology* **169**, 53. https://doi.org/10.1007/s00410-015-1141-8.

Hansteen, T. H. & Klügel, A. (2008). Fluid inclusion Thermobarometry as a tracer for magmatic processes. *Reviews in Mineralogy and Geochemistry* **69**, 143–177. https://doi.org/10.2138/rmg.2008.69.5.

Hansteen, T. H., Andersen, T., Neumann, E.-R. & Jelsma, H. (1991). Fluid and silicate glass inclusions in ultramafic and mafic xenoliths from Hierro, Canary Islands: implications for mantle metasomatism. *Contributions to Mineralogy and Petrology* **107**, 242–254. https://doi.org/10.1007/BF00310710.

Hansteen, T. H., Klügel, A. & Schmincke, H.-U. (1998). Multi-stage magma ascent beneath the Canary Islands: evidence from fluid inclusions. *Contributions to Mineralogy and Petrology* **132**, 48–64. https://doi.org/10.1007/s004100050404.

Hartley, M. E., Maclennan, J., Edmonds, M. & Thordarson, T. (2014). Reconstructing the deep CO2 degassing behaviour of large basaltic fissure eruptions. *Earth and Planetary Science Letters* **393**, 120–131. https://doi.org/10.1016/j.epsl.2014.02.031.

Helz, R. T., Clague, D. A., Sisson, T. W. & Thornber, C. R. (2014) Petrologic insights into basaltic volcanism at historically active Hawaiian volcanoes. In: *Characteristics of Hawaiian volcanoes*. US Geological Survey, Professional Papers, pp.237–294.

Hildner, E., Klügel, A. & Hauff, F. (2011). Magma storage and ascent during the 1995 eruption of Fogo, Cape Verde archipelago. *Contributions to Mineralogy and Petrology* **162**, 751–772. https://doi.org/10.1007/s00410-011-0623-6.

Hildner, E., Klügel, A. & Hansteen, T. H. (2012). Barometry of lavas from the 1951 eruption of Fogo, Cape Verde Islands: implications for historic and prehistoric magma plumbing systems. *Journal of Volcanology and Geothermal Research* **217-218**, 73–90. https://doi.org/10.1016/j.jvolgeores.2011.12.014.

Iacovino, K., Matthews, S., Wieser, P. E., Moore, G. M. & Bégué, F. (2021). VESIcal part I: an open-source thermodynamic model engine for mixed volatile (H2O-CO2) solubility in silicate melts. *Earth and Space Science* **8**, e2020EA001584. https://doi.org/10.1029/2020EA001584.

Kawakami, Y., Yamamoto, J. & Kagi, H. (2003). Micro-Raman Densimeter for $CO_2$ inclusions in mantle-derived minerals. *Applied Spectroscopy* **57**, 1333–1339. https://doi.org/10.1366/000370203322554473.

Kirby, S. H. & Green, H. W. (1980). Dunite xenoliths from Hualalai volcano: evidence for mantle diapiric flow beneath the island of Hawaii. *Amer J Sci A* **280**, 550–575.

Klügel, A., Hansteen, T. H. & Galipp, K. (2005). Magma storage and underplating beneath cumbre Vieja volcano, La Palma (Canary Islands). *Earth and Planetary Science Letters* **236**, 211–226. https://doi.org/10.1016/j.epsl.2005.04.006.

Klügel, A., Day, S., Schmid, M. & Faria, B. (2020). Magma plumbing during the 2014–2015 eruption of Fogo (Cape Verde Islands). *Frontiers in Earth Science* **8**, 157. https://doi.org/10.3389/feart.2020.00157.

Ladenberger, A., Lazor, P. & Michalik, M. (2009). CO2 fluid inclusions in mantle xenoliths from lower Silesia (SW Poland): formation conditions and decompression history. *European Journal of Mineralogy* **21**, 751–761. https://doi.org/10.1127/0935-1221/2009/0021-1930.

Lamadrid, H. M., Moore, L. R., Moncada, D., Rimstidt, J. D., Burruss, R. C. & Bodnar, R. J. (2017). Reassessment of the Raman CO2 densimeter. *Chemical Geology* **450**, 210–222. https://doi.org/10.1016/j.chemgeo.2016.12.034.

Le Maitre, R. W., Streckeisen, A., Zanettin, B., Le Bas, M. J., Bonin, B. & Bateman, P. (eds) (2002) *Igneous Rocks: A Classification and Glossary of Terms: Recommendations of the International Union of Geological Sciences Subcommission on the Systematics of Igneous Rocks*. Cambridge: Cambridge University Press.

Le, V.-H., Caumon, M.-C. & Tarantola, A. (2021). FRAnCIs calculation program with universal Raman calibration data for the determination of PVX properties of CO2–CH4–N2 and CH4–H2O–NaCl systems and their uncertainties. *Computers & Geosciences* **156**, 104896. https://doi.org/10.1016/j.cageo.2021.104896.

Lerner, A. H., Wallace, P. J., Shea, T., Mourey, A. J., Kelly, P. J., Nadeau, P. A., Elias, T., Kern, C., Clor, L. E., Gansecki, C., Lee, R. L., Moore, L. R. & Werner, C. A. (2021). The petrologic and degassing behavior of sulfur and other magmatic volatiles from the 2018 eruption of Kīlauea, Hawai'i: melt concentrations, magma storage depths, and magma recycling. *Bulletin of Volcanology* **83**, 1–32. https://doi.org/10.1007/s00445-021-01459-y.

Lerner, A. H., Sublett, D. M., Wallace, P. J., Cauley, C. & Bodnar, R. J. (2024). Insights into magma storage depths and eruption controls at Kīlauea volcano during explosive and effusive periods of the past 500 years based on melt and fluid inclusions. *Earth and Planetary Science Letters* **628**, 118579. https://doi.org/10.1016/j.epsl.2024.118579.

Levresse, G., Cervantes-de la Cruz, K. E., Aranda-Gómez, J. J., Dávalos-Elizondo, M. G., Jiménez-Sandoval, S., Rodríguez-Melgarejo, F. & Alba-Aldave, L. A. (2016). CO2 fluid inclusion barometry in mantle xenoliths from Central Mexico: a detailed record of magma ascent. *Journal of Volcanology and Geothermal Research* **310**, 72–88. https://doi.org/10.1016/j.jvolgeores.2015.11.012.

Liu, E. J., Cashman, K. V., Miller, E., Moore, H., Edmonds, M., Kunz, B. E., Jenner, F. & Chigna, G. (2020). Petrologic monitoring at Volcán de Fuego, Guatemala. *Journal of Volcanology and Geothermal Research* **405**, 107044. https://doi.org/10.1016/j.jvolgeores.2020.107044.

Lynn, K.J., Downs, D.T., Chang, J.M., Lundblad, S.P., Mills, P.R., McDade, B., Deligne, N.I., Gansecki, C.A., Schmith, J., Decker, M.F.I., Zoeller, M.H., Trusdell, F.A., Carr, B.B., Patrick, M.R., Parcheta, C., Nalesnik, A., Dietterich, H., Hazlett, R., Johnson, P.A., Gallant, E., Mulliken, K.M., Nadeau, P.A., Cappos, M.J., DeSmither, L., Peek, S., Damby, D., Dotray, P.J., van Helden, K.M., Shea, T., Hammer, J.E., Mourey, A.J., and Loewen, M.(2024a) Sample details and near-real-time ED-XRF data collected during the 2020-2023 Halema'uma'u eruptions of Kīlauea volcano, Island of Hawai'i: U.S. Geological Survey data release. https://doi.org/10.5066/P1XFKKYH

Lynn, K. J., Nadeau, P. A., Ruth, D. C. S., Chang, J. C., Dotray, P. J. & Johanson, I. A. (2024b). Olivine diffusion constrains months-scale magma transport within Kīlauea volcano's summit reservoir system prior to the 2020 eruption. *Bulletin of Volcanology* **86**, 31. https://doi.org/10.1007/s00445-024-01714-y.

Lynn, K. J., Downs, D. T., Trusdell, F. A., Wieser, P. E., Rangel, B., McDade, B., Hotovec-Ellis, A. J., Bennington, N., Anderson, K. R., Ruth, D. C. S., DeVitre, C. L., Ellis, A. P., Nadeau, P. A., Clor, L., Kelly, P., Dotray, P. J., & Chang, J. C. (2024c). Triggering the 2022 eruption of Mauna Loa. *Nature Communications* **15**(1), 9451. https://doi.org/10.1038/s41467-024-52881-7.

Mavrogenes, J. A. & Bodnar, R. J. (1994). Hydrogen movement into and out of fluid inclusions in quartz: experimental evidence and geologic implications. *Geochimica et Cosmochimica Acta* **58**, 141–148. https://doi.org/10.1016/0016-7037(94)90452-9.

Miyashiro, A. (1974). Volcanic rock series in island arcs and active continental margins. *American Journal of Science* **274**, 321–355. https://doi.org/10.2475/ajs.274.4.321.

Moore, L. R., Mironov, N., Portnyagin, M., Gazel, E. & Bodnar, R. J. (2018). Volatile contents of primitive bubble-bearing melt inclusions from Klyuchevskoy volcano, Kamchatka: comparison of volatile contents determined by mass-balance versus experimental homogenization. *Journal of Volcanology and Geothermal Research* **358**, 124–131. https://doi.org/10.1016/j.jvolgeores.2018.03.007.

Moore, L. R., Gazel, E. & Bodnar, R. J. (2021). The volatile budget of Hawaiian magmatism: constraints from melt inclusions from Haleakala volcano, Hawaii. *Journal of Volcanology and Geothermal Research* **410**, 107144. https://doi.org/10.1016/j.jvolgeores.2020.107144.

Mourey, A. J., Shea, T., Costa, F., Shiro, B. & Longman, R. J. (2023). Years of magma intrusion primed Kīlauea volcano (Hawai'i) for the 2018 eruption: evidence from olivine diffusion chronometry and monitoring data. *Bulletin of Volcanology* **85**, 18. https://doi.org/10.1007/s00445-023-01633-4.

Pankhurst, M. J., Scarrow, J. H., Barbee, O. A., Hickey, J., Coldwell, B. C., Rollinson, G. K., Rodríguez-Losada, J. A., Martín Lorenzo, A., Rodríguez, F., Hernández, W., Calvo Fernández, D., Hernández, P. A. & Pérez, N. M. (2022). Rapid response petrology for the opening eruptive phase of the 2021 cumbre Vieja eruption, La Palma, Canary Islands. *Volcanica* **5**, 1–10. https://doi.org/10.30909/vol.05.01.0110.

Pietruszka, A. J., Heaton, D. E., Marske, J. P. & Garcia, M. O. (2015). Two magma bodies beneath the summit of Kīlauea volcano unveiled by isotopically distinct melt deliveries from the mantle. *Earth and Planetary Science Letters* **413**, 90–100. https://doi.org/10.1016/j.epsl.2014.12.040.

Pietruszka, A. J., Marske, J. P., Heaton, D. E., Garcia, M. O. & Rhodes, J. M. (2018). An isotopic perspective into the magmatic evolution and architecture of the rift zones of Kīlauea volcano. *Journal of Petrology* **59**, 2311–2352. https://doi.org/10.1093/petrology/egy098.

Pritchard, M. E., Mather, T. A., McNutt, S. R., Delgado, F. J. & Reath, K. (2019). Thoughts on the criteria to determine the origin of volcanic unrest as magmatic or non-magmatic. *Philosophical Transactions of the Royal Society A* **377**, 20180008. https://doi.org/10.1098/rsta.2018.0008.

Re, G., Corsaro, R. A., D'Oriano, C. & Pompilio, M. (2021). Petrological monitoring of active volcanoes: a review of existing procedures to achieve best practices and operative protocols during eruptions. *Journal of Volcanology and Geothermal Research* **419**, 107365. https://doi.org/10.1016/j.jvolgeores.2021.107365.

Roedder, E. (1965). Liquid CO2 inclusions in olivine-bearing nodules and phenocrysts from basalts. *American mineralogist: journal of earth and planetary materials. Mineralogical Society of America* **50**, 1746–1782.

Roedder, E. (1983). Geobarometry of ultramafic xenoliths from Loihi seamount, Hawaii, on the basis of CO2 inclusions in olivine. *Earth and Planetary Science Letters* **66**, 369–379. https://doi.org/10.1016/0012-821X(83)90152-8.

Roedder, E. (1984) *Fluid Inclusions (Reviews in Mineralogy vol. 12)*. Washington DC: Mineralogical Society of America.

Roedder, E. & Bodnar, R. J. (1980). Geologic pressure determinations from fluid inclusion studies. *Annual Review of Earth and Planetary Sciences* **8**, 263–301. https://doi.org/10.1146/annurev.ea.08.050180.001403.

Rosso, K. M. & Bodnar, R. J. (1995). Microthermometric and Raman spectroscopic detection limits of C02 in fluid inclusions and the Raman spectroscopic characterization of C02. *Geochimica et Cosmochimica Acta* **59**, 3961–3975. https://doi.org/10.1016/0016-7037(95)94441-H.

Ryan, M. P. (1987). The elasticity and contractancy of Hawaiian olivine tholeiite, and its role in the stability and structural evolution of sub-caldera magma reservoirs and rift systems. In volcanism in Hawaii. *US Geol. Surv. Prof. Pap.* **1350**, 1395–1447.

Sendula, E., Lamadrid, H. M., Rimstidt, J. D., Steele-MacInnis, M., Sublett, D. M., Aradi, L. E., Szabó, C., Caddick, M. J., Zajacz, Z. & Bodnar, R. J. (2021). Synthetic Fluid Inclusions XXIV. In situ Monitoring of the Carbonation of Olivine Under Conditions Relevant to Carbon Capture and Storage Using Synthetic Fluid Inclusion Micro-Reactors: Determination of Reaction Rates. *Frontiers in Climate* **3**, 722447. https://doi.org/10.3389/fclim.2021.722447.

Span, R. & Wagner, W. (1996). A new equation of state for carbon dioxide covering the fluid region from the triple-point temperature to 1100 K at pressures up to 800 MPa. *Journal of Physical and Chemical Reference Data* **25**, 1509–1596. https://doi.org/10.1063/1.555991.

Sterner, S. M. & Bodnar, R. J. (1989). Synthetic fluid inclusions - VII. Re-equilibration of fluid inclusions in quartz during laboratory-simulated metamorphic burial and uplift. *Journal of Metamorphic Geology* **7**, 243–260. https://doi.org/10.1111/j.1525-1314.1989.tb00587.x.

Sublett, D. M., Sendula, E., Lamadrid, H., Steele-MacInnis, M., Spiekermann, G., Burruss, R. C. & Bodnar, R. J. (2020). Shift in the Raman symmetric stretching band of N2, CO2, and CH4 as a function of temperature, pressure, and density. *Journal of Raman Spectroscopy* **51**, 555–568. https://doi.org/10.1002/jrs.5805.

Swanson, D. A., Rose, T. R., Mucek, A. E., Garcia, M. O., Fiske, R. S. & Mastin, L. G. (2014). Cycles of explosive and effusive eruptions at Kīlauea volcano, Hawai'i. *Geology* **42**, 631–634. https://doi.org/10.1130/G35701.1.

Taracsák, Z., Hartley, M. E., Burgess, R., Edmonds, M., Iddon, F. & Longpré, M.-A. (2019). High fluxes of deep volatiles from ocean island volcanoes: insights from El Hierro, Canary Islands. *Geochimica et Cosmochimica Acta* **258**, 19–36. https://doi.org/10.1016/j.gca.2019.05.020.

Venugopal, S., Moune, S., Williams-Jones, G., Druitt, T., Vigouroux, N., Wilson, A. & Russell, J. K. (2020). Two distinct mantle sources beneath the Garibaldi Volcanic Belt: insight from olivine-hosted melt inclusions. *Chemical Geology* **532**, 119346. https://doi.org/10.1016/j.chemgeo.2019.119346.

Viti, C. & Frezzotti, M.-L. (2000). Re-equilibration of glass and CO2 inclusions in xenolith olivine: a TEM study. *American Mineralogist* **85**, 1390–1396. https://doi.org/10.2138/am-2000-1007.

Wanamaker, B. J. & Evans, B. (1989). Mechanical re-equilibration of fluid inclusions in San Carlos olivine by power-law creep. *Contributions to Mineralogy and Petrology* **102**, 102–111. https://doi.org/10.1007/BF01160194.

Wang, X., Chou, I.-M., Hu, W., Burruss, R. C., Sun, Q. & Song, Y. (2011). Raman spectroscopic measurements of CO2 density: experimental calibration with high-pressure optical cell (HPOC) and fused silica capillary capsule (FSCC) with application to fluid inclusion observations. *Geochimica et Cosmochimica Acta* **75**, 4080–4093. https://doi.org/10.1016/j.gca.2011.04.028.

Wang, W., Caumon, M.-C., Tarantola, A., Pironon, J., Lu, W. & Huang, Y. (2019). Raman spectroscopic densimeter for pure CO2 and CO2-H2O-NaCl fluid systems over a wide P-T range up to 360 °C and 50 MPa. *Chemical Geology* **528**, 119281. https://doi.org/10.1016/j.chemgeo.2019.119281.

Welsch, B., Faure, F., Famin, V., Baronnet, A. & Bachèlery, P. (2013). Dendritic crystallization: a single process for all the textures of olivine in basalts? *Journal of Petrology* **54**, 539–574. https://doi.org/10.1093/petrology/egs077.

Wieser, P. E. & DeVitre, C. (2024). DiadFit: an open-source Python3 tool for peak fitting of Raman data from silicate melts and CO2 fluids. *Volcanica* **7**, 335–359. https://doi.org/10.30909/vol.07.01.335359.

Wieser, P. E., Edmonds, M., Maclennan, J., Jenner, F. E. & Kunz, B. E. (2019). Crystal scavenging from mush piles recorded by melt inclusions. *Nature Communications* **10**, 5797. https://doi.org/10.1038/s41467-019-13518-2.

Wieser, P. E., Lamadrid, H., Maclennan, J., Edmonds, M., Matthews, S., Iacovino, K., Jenner, F. E., Gansecki, C., Trusdell, F., Lee, R. L. & Ilyinskaya, E. (2021). Reconstructing magma storage depths for the 2018 Kı̄lauean eruption from melt inclusion CO2 contents: the importance of vapor bubbles. *Geochemistry, Geophysics, Geosystems* **22**, e2020GC009364. https://doi.org/10.1029/2020GC009364.

Wieser, P. E., Kent, A. J. R. & Till, C. B. (2023a). Barometers behaving badly II: a critical evaluation of Cpx-only and Cpx-Liq Thermobarometry in variably-hydrous arc magmas. *Journal of Petrology* **64**, 1–25, egad050. https://doi.org/10.1093/petrology/egad050.

Wieser, P. E., Kent, A. J. R., Till, C. B. & Abers, G. A. (2023). Geophysical and Geochemical Constraints on Magma Storage Depths Along the Cascade Arc: Knowns and Unknowns. *Geochemistry, Geophysics, Geosystems* **24**(11), e2023GC011025. https://doi.org/10.1029/2023GC011025.

Wieser, P. E., Gleeson, M. L. M., Matthews, S., DeVitre, C. & Gazel, E. (2025). Determining the pressure-temperature-composition (P-T-X) conditions of magma storage. In A. Anbar & D. Weis (Eds.), *Treatise on Geochemistry (Third edition)*, (pp. 83–151). Elsevier, Oxford. https://doi.org/10.1016/B978-0-323-99762-1.00024-3.

Wong, K., Ferguson, D., Wieser, P., Morgan, D., Edmonds, M., Tadesse, A. Z., Yirgu, G., Harvey, J. & Hammond, S. (2023). Focused mid-crustal magma intrusion during continental break-up in Ethiopia. *Geophysical Research Letters* **50**, e2023GL103257. https://doi.org/10.1029/2023GL103257.

Yamamoto, J. & Kagi, H. (2006). Extended micro-Raman densimeter for CO2 applicable to mantle-originated fluid inclusions. *The Chemical Society of Japan* **35**, 610–611.

Yamamoto, J., Kagi, H., Kaneoka, I., Lai, Y., Prikhod'ko, V. S. & Arai, S. (2002). Fossil pressures of fluid inclusions in mantle xenoliths exhibiting rheology of mantle minerals: implications for the geobarometry of mantle minerals using micro-Raman spectroscopy. *Earth and Planetary Science Letters* **198**, 511–519. https://doi.org/10.1016/S0012-821X(02)00528-9.

Yamamoto, J., Kagi, H., Kawakami, Y., Hirano, N. & Nakamura, M. (2007). Paleo-Moho depth determined from the pressure of CO2 fluid inclusions: Raman spectroscopic barometry of mantle- and crust-derived rocks. *Earth and Planetary Science Letters* **253**, 369–377. https://doi.org/10.1016/j.epsl.2006.10.038.

Yamamoto, J., Otsuka, K., Ohfuji, H., Ishibashi, H., Hirano, N. & Kagi, H. (2011). Retentivity of CO2 in fluid inclusions in mantle minerals. *European Journal of Mineralogy* **23**, 805–815. https://doi.org/10.1127/0935-1221/2011/0023-2150.

Yoshimura, S. (2023). Carbon dioxide and water in the crust. Part 1: equation of state for the fluid. *Journal of Mineralogical and Petrological Sciences* **118**, 221224a.

Zanon, V. & Frezzotti, M. L. (2013). Magma storage and ascent conditions beneath Pico and Faial islands (Azores archipelago): a study on fluid inclusions. *Geochemistry, Geophysics, Geosystems* **14**, 3494–3514. https://doi.org/10.1002/ggge.20221.

Zanon, V., Frezzotti, M.-L. & Peccerillo, A. (2003). Magmatic feeding system and crustal magma accumulation beneath Vulcano Island (Italy): evidence from CO2 fluid inclusions in quartz xenoliths. *Journal of Geophysical Research: Solid Earth* **108**(B6), 2298. https://doi.org/10.1029/2002JB002140.

Zanon, V., D'Auria, L., Schiavi, F., Cyrzan, K. & Pankhurst, M. J. (2024). Toward a near real-time magma ascent monitoring by combined fluid inclusion barometry and ongoing seismicity. *Science advances*. American association for the. *Advancement of Science* **10**, eadi4300. https://doi.org/10.1126/sciadv.adi4300.



Published by Oxford University Press 2024. This work is written by US Government employees and is in the public domain in the US.
*Journal of Petrology*, 2024, **65**, egae119
https://doi.org/10.1093/petrology/egae119
Original Manuscript